Detection of morphological markers of vulnerable atherosclerotic plaque using multimodal spectroscopy

Obrad R. Šćepanović
Massachusetts Institute of Technology
G. R. Harrison Spectroscopy Laboratory
Cambridge, Massachusetts 02139
E-mail: obrad@mit.edu

Maryann Fitzmaurice
University Hospitals of Cleveland
and
Case Western Reserve University
Cleveland, Ohio

Joseph A. Gardecki
George O. Angheloiu
Samir Awasthi
Massachusetts Institute of Technology
G. R. Harrison Spectroscopy Laboratory
Cambridge, Massachusetts 02139

Jason T. Motz
Massachusetts General Hospital
Wellman Center for Photomedicine
Boston, Massachusetts

John R. Kramer
Ramachandra R. Dasari
Michael S. Feld
Massachusetts Institute of Technology
G. R. Harrison Spectroscopy Laboratory
Cambridge, Massachusetts 02139

Abstract. Vulnerable plaques, which are responsible for most acute ischemic events, are presently invisible to x-ray angiography. Their primary morphological features include a thin or ulcerated fibrous cap, a large necrotic core, superficial foam cells, and intraplaque hemorrhage. We present evidence that multimodal spectroscopy (MMS), a novel method that combines diffuse reflectance spectroscopy (DRS), intrinsic fluorescence spectroscopy (IFS), and Raman spectroscopy (RS), can detect these markers of plaque vulnerability. To test this concept, we perform an MMS feasibility study on 17 human carotid artery specimens. Following the acquisition of spectra, each specimen is histologically evaluated. Two parameters from DRS, hemoglobin concentration and a scattering parameter, are used to detect intraplaque hemorrhage and foam cells; an IFS parameter that relates to the amount of collagen in the topmost layers of the tissue is used to detect the presence of a thin fibrous cap; and an RS parameter related to the amount of cholesterol and necrotic material is used to detect necrotic core. Taken together, these spectral parameters can generally identify the vulnerable plaques. The results indicate that MMS provides depth-sensitive and complementary morphological information about plaque composition. A prospective *in vivo* study will be conducted to validate these findings. [DOI: 10.1117/1.2187943]

Keywords: atherosclerosis; vulnerable plaque; morphology; spectroscopy; multimodal.

Paper 05172SSR received Jul. 2, 2005; revised manuscript received Nov. 29, 2005; accepted for publication Dec. 22, 2005; published online Mar. 27, 2006.

1 Introduction

The severity of atherosclerotic lesions has traditionally been assessed by imaging their location and percentage of intraluminal stenosis. However, landmark studies over the past ten years have shown that up to 70% of acute cardiac ischemic events result from the rupture of previously subsymptomatic lesions, ending in thrombotic occlusion and, often, myocardial infarction.[1,2] The vast majority of these thrombosed coronary artery plaques exhibit less than 75% stenosis,[3] the figure often used to define a clinically significant lesion. Thus, plaques that are not critically stenotic can still cause acute ischemic events.[4,5]

These vulnerable plaques often exhibit rupture of a so-called thin cap fibrous atheroma, i.e., a plaque with a thin ($<65\ \mu$m) fibrous cap overlying a large (>2 mm) necrotic core.[3] A recent consensus paper by cardiovascular pathologists[6] has reported that additional morphological features may be associated with thrombosis, such as erosion or denudation of the intimal endothelial layer. In both ruptured and eroded plaques, the fibrous cap[2,3] or superficial intima[5] is frequently infiltrated by inflammatory cells, most often macrophages and foam cells. Exposed calcifications[3] and acute intraplaque hemorrhage or dissection[2] are other common features of thrombosed plaques.

There is currently great interest in developing new techniques for clinical imaging of vulnerable plaque, including advances in intravascular ultrasound, optical coherence tomography, and thermography.[7] Optical spectroscopy is also being studied for evaluation of these critical lesions. Several groups have explored the use of near-infrared spectroscopy to characterize atherosclerotic plaque,[8,9] with a recent paper reporting promising results in detecting markers of plaque vulnerability.[10] Fluorescence spectroscopy has also shown potential to detect features of vulnerable plaque, including a thin fibrous cap.[11]

The present work explores the potential of combining complementary spectroscopic methods, reflectance, fluorescence, and Raman spectroscopy to evaluate the morphological

Address all correspondence to Obrad R. Šćepanović, Massachusetts Institute of Technology, G. R. Harrison Spectroscopy Laboratory, 77 Massachusetts Ave., Room NW14–1106, Cambridge, Massachusetts 02139. Tel: 617–253–5766; Fax: 617–253–4513; E-mail: obrad@mit.edu

1083-3668/2006/11(2)/021007/9/$22.00 © 2006 SPIE

features of atherosclerotic plaque and assess plaque vulnerability, particularly by the detection of intraplaque hemorrhage, density and depth of superficial foam cells, fibrous cap thickness, and necrotic core size. This combination provides both depth sensitivity, important for identifying thin fibrous caps, and complementary morphological information. We term this method multimodal spectroscopy (MMS).

Using diffuse reflectance spectroscopy (DRS), we study the spectrum of near-UV-visible light (300 to 700 nm) traversing turbid biological tissue. The resulting spectrum exhibits features due to scattering and absorption of the incident light by the tissue. We have developed a model to analyze DRS spectra based on an analytical expression for diffusion of multiply scattered light to extract the wavelength-dependent coefficients of scattering and absorption.[12] In atherosclerotic plaque, the main absorbers are hemoglobin, associated with thrombus or acute intraplaque hemorrhage, and beta-carotene, whose absorption has been used previously for spectroscopic detection of atherosclerosis in an animal model.[13]

Fluorescence spectroscopy relies on the excitation of molecular electronic energy levels, giving rise to re-emission at wavelengths longer than the exciting light. The emission spectrum provides information about the fluorophores excited. The primary fluorophores in arterial tissue are elastin, collagen, tryptophan, ceroid,[14] and oxidized low-density lipoprotein (LDL).[11] A number of research groups, including our own, have employed continuous wave[11,15–22] and time-resolved[23,24] fluorescence spectroscopy to diagnose atherosclerosis. However, the broad overlapping spectral features of tissue fluorophores, further confounded by absorption and scattering, are a barrier to extracting spectral information with sufficient accuracy for quantitative analysis of vulnerable plaque. One recent study using fluorescence showed promising results in identifying thin fibrous cap atheromas, but a number of samples had to be eliminated from the analysis due to the inability to compensate for the spectral distortions caused by scattering and absorption.[11] We have developed a method to remove these distortions using the information from the DRS spectrum, and thus extract the intrinsic fluorescence,[25,26] which can be decomposed into a linear combination of the spectra from fluorophores associated with morphological structures in the tissue. Intrinsic fluorescence spectroscopy (IFS) has been successfully employed in our research for cancer diagnosis.[27,28]

Raman spectroscopy (RS) detects molecules by exciting vibrations among bonds that are unique to each molecule, and has been used extensively in biomedicine.[29,30] Previous work by our group on RS of atherosclerosis identified eight key morphological components in arterial pathogenesis that could be identified by their Raman spectral signatures: collagen fibers (CF), cholesterol crystals (CC), calcium mineralization (CM), elastic lamina (EL), adventitial adipocytes (AA), foam cells/necrotic core (FC/NC), beta-carotene crystals (β-CC), and smooth muscle cells (SMC).[31] A diagnostic algorithm, using morphological information extracted with a linear combination model similar to that used for IFS, is able to classify *in vitro* coronary artery specimens as nonatherosclerotic, noncalcified plaque and calcified plaque with 94% accuracy.[32] The development of a small-diameter, high-throughput, filtered Raman probe[33] has resulted in the first *in vivo* clinical application of the RS diagnostic algorithm in real time during carotid endarterectomy and femoral bypass surgery.[34–36]

MMS, the combined use of DRS, IFS, and RS, yields complementary biochemical and morphological information about arterial tissue that no individual modality can provide by itself. Furthermore, the information obtained by these modalities is depth-sensitive due to the inherently different tissue penetration by the various incident wavelengths employed. The results of the following feasibility study indicate that MMS has the potential to accurately assess plaque vulnerability *in vivo*, in real time, and as a guide to future treatment.

2 Methods

2.1 *Depth Sensing*

Light of different wavelengths penetrates tissue to different depths. The effective penetration depth is defined as the depth at which the power of light incident on a tissue sample falls to 1/e of its incident value, and can be calculated from diffusion theory:

$$\delta = \frac{1}{\mu_{\text{eff}}} = \frac{1}{[3\mu_a(\mu_a + \mu_s')]^{1/2}},$$

using the values for the reduced scattering coefficient μ_s' and absorption coefficient μ_a of tissue. Based on this equation, the literature on the optical properties of aorta indicates effective penetration depths of about 90, 140, and 1200 μm for light of wavelengths 308, 340, and 830 nm, respectively.[37] Another study indicates values 70, 90, and 800 μm for the effective penetration depths of 308, 340, and 830 nm in aortic tissue.[38]

We performed experiments to verify these values using our instruments and probes. The penetration depths at different excitation wavelengths were measured by incrementally stacking 20-μm-thick sections of aortic media. An optical fiber probe, placed in contact with the tissue, delivered the light, and a power meter measured the transmitted power as a function of tissue thickness. Note that in the single-ended geometry of our artery studies (i.e., the probe both delivers and collects light from the same side of the tissue), we need to account for the propagation of both the excitation and emission light. Thus the sampling depth δ_s can be related by

$$\frac{1}{\delta_s} = \frac{1}{\delta_{\text{ex}}} + \frac{1}{\delta_{\text{em}}},$$

where δ_{ex} and δ_{em} are the penetration depths of the excitation and emission light, respectively. Other groups have defined the sampling depth, or probing depth, as the depth above which 90% of the remitted fluorescence originates.[39]

2.2 *Tissue Study*

We have performed a preliminary *in vitro* study to establish the effectiveness of DRS, IFS, and RS for providing information about plaque morphology and vulnerability. Spectra were collected from excised human carotid endarterectomy specimens (n=17) from 12 patients, obtained from the Cooperative Human Tissue Network. The snap-frozen specimens were thawed and rinsed in phosphate-buffered saline. The DRS and IFS spectra were obtained using a fast excitation-emission matrix (FastEEM) instrument and probe, described in detail elsewhere.[40,41] The FastEEM probe was placed in gentle con-

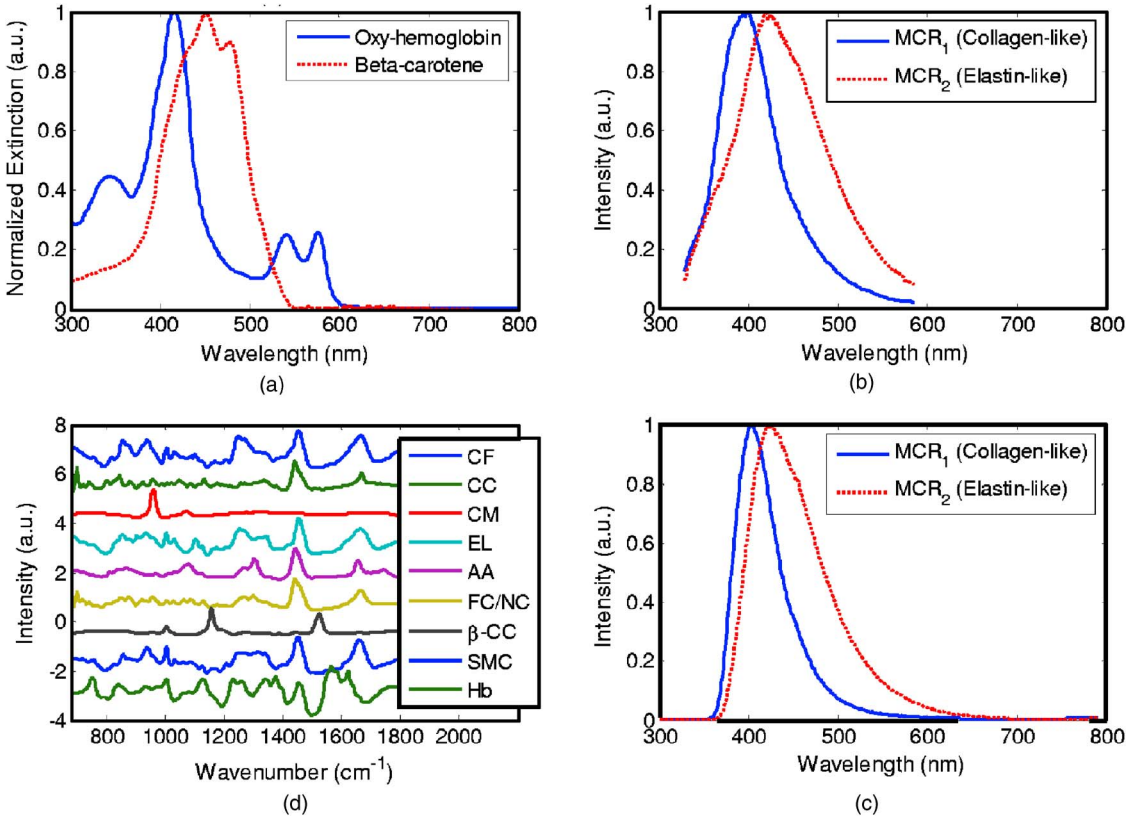

Fig. 1 (a) Extinction coefficients of oxy-hemoglobin and beta-carotene; (b) MCR basis spectra components for IFS at 308 nm; (c) the MCR basis spectra components for IFS at 340 nm; and (d) Raman morphological model basis spectra.

tact with the intimal layer of the tissue while DRS and IFS spectra were collected (1-s total acquisition time). The RS signal was then acquired from the same location using a clinical Raman system and probe, described elsewhere[33–36] (1- to 5-s total acquisition time). Care was taken to insure the placement of the probes on the same tissue location.

Following spectral acquisition, the evaluation site was demarcated with India ink and the specimen was fixed in formalin, routinely processed, sectioned, and stained with hematoxylin and eosin. Histopathology for each of the 17 specimens was performed by an experienced cardiovascular pathologist (MF) blinded to the spectroscopy results. The morphological features associated with plaque vulnerability were assessed: fibrous cap thickness, necrotic core size, superficial foam cells, intraplaque hemorrhage, and ulceration. The intimal or fibrous cap thickness was recorded as the range of thicknesses found underneath the ink dot. The necrotic core size was recorded as the maximum dimension of the core beneath the fibrous cap, if present. The foam cells were evaluated based on the most superficial depth at which they were found and a density grade (0=none; 1+=isolated single foam cells; 2+=small clusters of foam cells; 3+=confluent sheets of foam cells). Intraplaque hemorrhage was identified as an accumulation of blood within the lesion, usually associated with the core. Plaque ulceration was graded based on whether the defect in the fibrous cap did (rupture) or did not extend (fissure) into the underlying atheroma core.

DRS spectra were used to extract the wavelength-dependent absorption coefficient $\mu_a(\lambda)$ and reduced scattering coefficient $\mu_s'(\lambda)$ based on a diffusion theory model.[12] We modeled $\mu_a(\lambda)$ as a linear combination of two absorbers, oxy-hemoglobin and β-carotene:

$$\mu_a(\lambda) = [Hb]^* \varepsilon_{Hb}(\lambda) + [\beta c]^* \varepsilon_{\beta c}(\lambda),$$

with $[Hb]$ and $[\beta c]$ the concentrations and $\varepsilon_{Hb}(\lambda)$ and $\varepsilon_{\beta c}(\lambda)$ the extinction coefficients of oxy-hemoglobin and β-carotene, respectively [Fig. 1(a)]. Deoxy-hemoglobin was not included in the model because this is an *in vitro* study of frozen-thawed tissues in which the hemoglobin was oxygenated by exposure to room air. We modeled the $\mu_s'(\lambda)$ spectrum as an inverse power law, $\mu_s'(\lambda)=A\lambda^{-B}$, as reported elsewhere.[42,43]

IFS spectra were obtained by correcting the raw fluorescence for the effects of scattering and absorption.[25,26] Based on literature values, IFS spectra excited at 308 and 340 nm have the shallowest sampling depths and were used to assess the composition of the fibrous cap. Multivariate curve resolution (MCR), a chemometric technique used to extract the individual spectra of a known number of components from a mixture spectrum,[44] was performed on the IFS spectra at each of the two excitation wavelengths. For IFS at 308 and 340 nm, a linear combination of two MCR components [MCR_1 and MCR_2, Figs. 1(b) and 1(c)] resulted in good fits to all 17 spectra. The fit coefficient of the blue-shifted and narrower MCR component (MCR_1) is reported as C_{308} and C_{340} for IFS at 308 and 340 nm, respectively.

Raman spectra were fit using a linear combination of basis spectra components of the eight morphological structures (CF,

Table 1 Morphological features of the 17 specimens. IF=intimal fibroplasias, ATS=atherosclerotic plaque, ATM=atheromatous plaque, FS=fibrotic-sclerotic plaque, C=calcified.

Specimen number	SNOMed classification	Intimal or fibrous cap thickness (microns)	Necrotic core thickness (microns)	Foam cell depth (microns)	Foam cell grade (0–3+)	Intraplaque hemorrhage	Ulceration
1	IF	24 to 64	—	—	—	—	—
2	IF	40 to 80	—	—	—	—	—
3	ATS	480 to 500	—	480	3+	—	—
4	ATS	240 to 440	—	40	1+	—	—
5	ATS	456 to 536	—	456	2+	—	—
6	ATM	200 to 320	400	280	2+	—	—
7	ATM	460 to 640	560	—	—	—	—
8	ATM	440 to 500	4800	440	2+	—	—
9	ATM	1000 to 1500	6400	1800	1+	—	—
10	ATM	520 to 640	1340	640	2+	—	—
11	CATM	140 to 160	1840	68	1+	—	—
12	CATM	120 to 480	4000	120	1+	—	—
13	CATM	1440 to 1600	240	256	1+	—	—
14	CFS	0 to 400	—	—	—	Acute	Fissure
15	FS	40 to 80	—	—	—	—	Rupture
16	ATS	27 to 52	—	0	1+	—	—
17	ATM	0 to 280	1600	28	2+	—	Rupture

CC, CM, EL, AA, FC/NC, β-CC, and SMC) and hemoglobin [Fig. 1(d)]. The Raman fit coefficients were normalized to sum to unity so that each fit coefficient specifies a percentage contribution to the fit by that respective basis spectrum, as previously described.[32,34,45] The hemoglobin contribution to the Raman spectra was zero in all of our samples, as hemoglobin is a relatively weak Raman scatterer at 830-nm excitation. The spectral parameters obtained were then correlated with the presence (or absence) of the morphologic features of vulnerable plaque.

3 Results

3.1 *Depth Sensing*

In our experiments, the effective penetration depths at 308 and 340 nm were measured as 85 and 105 μm, respectively. The corresponding fluorescence emission peaks were 400 and 410 nm, respectively, with effective penetration depths of 128 and 147 μm. Therefore, the sampling depths for the IFS at 308 and 340 nm are 51 and 62 μm, respectively, accounting for the longer emission wavelength of the fluorescent light. Similarly, there were different wavelength regions of the DRS spectra sample tissue at different depths (50 to 500 μm). A previous experiment estimated the sampling depth of 470 μm for 830-nm Raman excitation.[35] The prior penetration depths, measured on aortic media, may vary with different types of lesions. Nevertheless, the trend of deeper sampling depth for longer wavelength excitation light still holds for each sample or atherosclerotic lesion.

3.2 *Tissue Study*

The histopathologic parameters relating to plaque vulnerability are summarized in Table 1 for each of the 17 specimens. The last four specimens exhibit the hallmarks of vulnerable plaque and are so classified: specimen 14 contains an intraplaque hemorrhage, specimens 15, 16, and 17 all have thin fibrous caps, some with presence of ulceration, superficial foam cells, and necrotic core. The remaining specimens (1 through 13) do not have the necessary combination of features to be deemed vulnerable.

Figure 1 shows the model components: oxy-hemoglobin and β-carotene extinction spectra (DRS), MCR components for IFS at 308 and 340 nm, and RS morphological basis spectra. Representative MMS spectra from the three modalities are shown in Fig. 2(a) for intimal fibroplasia, Fig. 2(b) for nonvulnerable atherosclerotic plaque, and Fig. 2(c) vulnerable

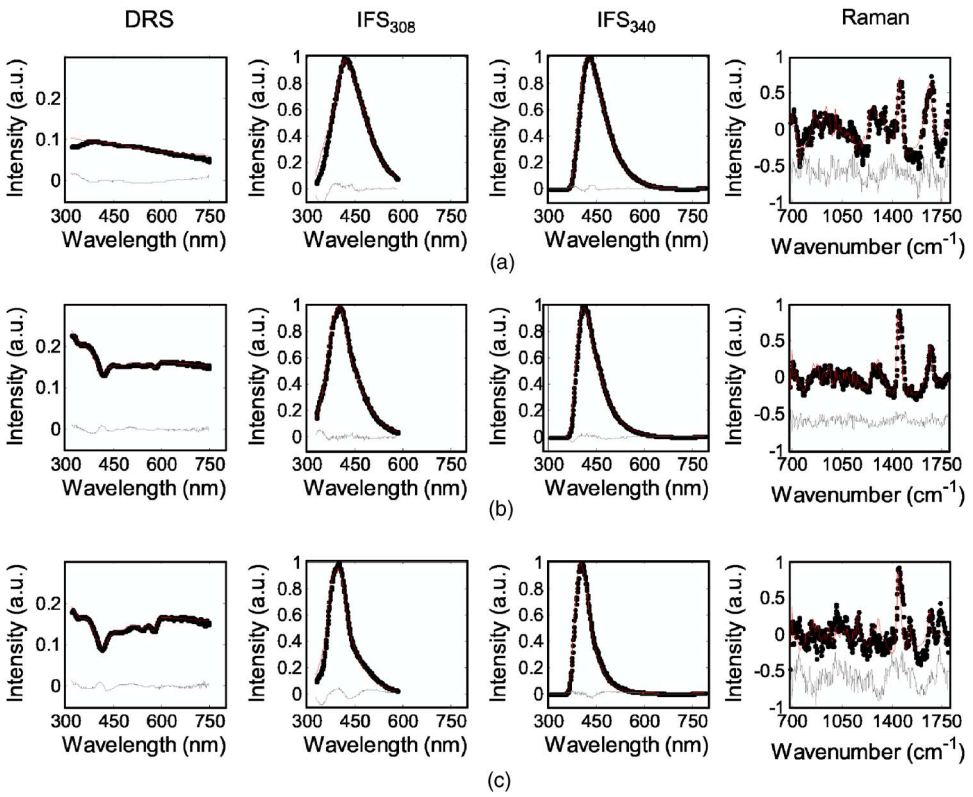

Fig. 2 Representative spectra (dotted black line), fits (solid red line) (color online only), and residuals between the data and fit (lowermost gray line) of the MMS modalities for three specimens with different pathologies: (a) intimal fibroplasia; (b) atherosclerotic plaque (not vulnerable); and (c) vulnerable atheromatous plaque. Note the progression of an increased presence of hemoglobin (420-nm absorption dip in DRS) for the three specimens. The IFS spectra for intimal fibroplasia are broader (characteristic of elastin) when compared to the more narrow spectra for the plaques (characteristic of collagen in the fibrous cap). The Raman spectrum of (c) is noisy due to the decreased signal intensity associated with hemoglobin absorption.

atheromatous plaque. The difference between the measured spectrum and the model fit, the residual, is shown below each spectrum. Lack of significant structure in the residuals demonstrates that the model accounts for the majority of spectroscopic features observed and robustly describes the data.

The following spectroscopic parameters showed the best correlation with morphologic features of vulnerable plaque: DRS hemoglobin concentration $[Hb]$, DRS scattering parameter A, IFS parameter $\rho = C_{308}/C_{340}$, and Raman parameter $\Sigma = CC + FC/NC$.

The DRS spectra are composed of contributions from absorption and scattering. The absorption is primarily due to oxy-hemoglobin, with a small contribution due to β-carotene. The scattering parameter A is related to the total amount of scattering produced by the tissue. The parameters $[Hb]$ and A are given in Figs. 3(a) and 3(b), respectively, for the 17 specimens.

Components MCR_1 and MCR_2 of IFS at both 308 and 340 nm (Fig. 1) exhibit features similar to the IFS spectra of collagen and elastin, respectively, as reported in previous studies at similar excitation wavelengths.[11,17,20] Both IFS MCR_1 and the fluorescence spectrum of collagen are blue shifted and more narrow when compared to IFS MCR_2 and the fluorescence spectrum of elastin, which has a longer tail. Thus, we conclude that the corresponding fit coefficients C_{308} and C_{340} of MCR_1 are related to the amount of collagen present within the tissue volume sampled. We define an IFS parameter ρ as the ratio of the fit coefficients of MCR_1 at 308- and 340-nm excitation ($\rho = C_{308}/C_{340}$), which is related to the amount of collagen present and the depth at which it is found. Since the sampling depth at 340-nm excitation is greater than that at 308 nm (see Depth Sensing in Sec. 3.1), C_{340} provides information about collagen distributed over a greater depth compared to that provided by C_{308}. Values of ρ are shown in Fig. 3(c) for each of the specimens. A value of ρ was undefined for specimen 1, as C_{340} was smaller than the error in this case (see Error Analysis in Sec. 3.3), implying a potential division by zero.

Previous diagnostic algorithms[32] were able to discriminate plaque content using the sum of the Raman fit coefficients for CC and FC/NC. Similarly, we defined a parameter $\Sigma = CC + FC/NC$, which is given for each specimen in Fig. 3(d). We use Σ to measure the presence of necrotic core.

3.3 *Error Analysis*

To determine the error in our spectral parameters, we performed a chi-square analysis and applied the error propagation formula.[46] Chi-square-analysis is a standard method for calculating the goodness of a fit and the error associated with fitting parameters. Errors reported for ρ and Σ are based on

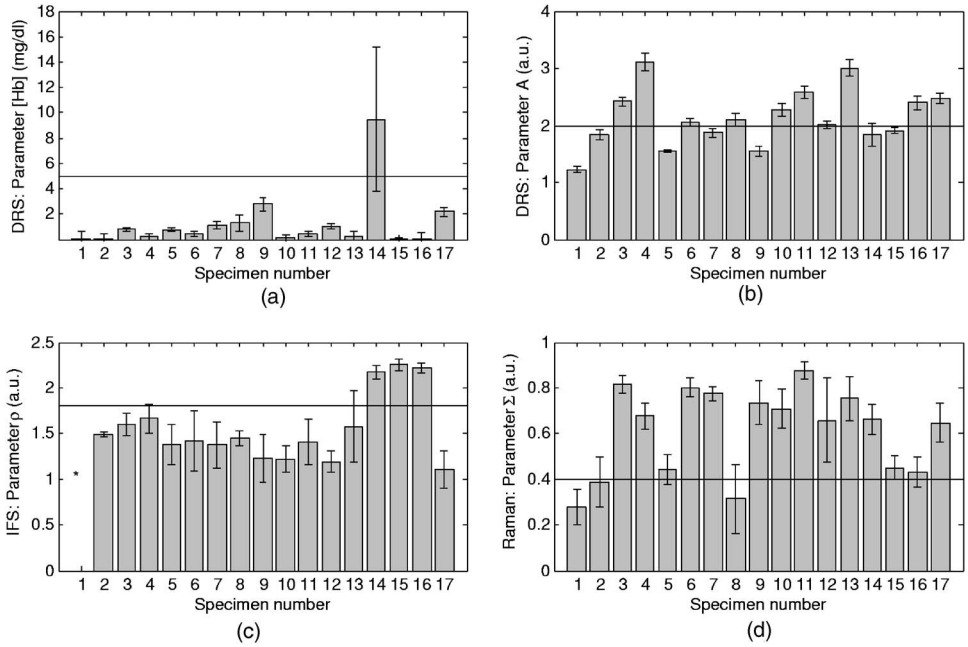

Fig. 3 Spectral parameters for each of the 17 specimens: (a) hemoglobin concentration (mg/mL) obtained from DRS, used to detect intraplaque hemorrhage; (b) scattering parameter A (relative units) obtained from DRS, used to detect the presence of foam cells; (c) ρ parameter (relative units) extracted from IFS_{340} and IFS_{308}, used to detect a thin fibrous cap [the value of ρ for specimen 1 (*) is undefined as C_{340} is within the error for this sample]; and (d) the Σ parameter (relative units) extracted from the Raman fit coefficients, used to obtain information about the presence of necrotic core. The error bars indicate one standard deviation.

propagating error from the individual components. The error bars in Fig. 3 are generated from this analysis.

4 Discussion

We compare the extracted spectroscopic parameters with the measured morphologic features, and demonstrate how the former can be used to make inferences about the latter, and thus serve to characterize plaque vulnerability. The small size of this sample set is somewhat offset by our ability to directly compare spectroscopic features with those of pathology.

Intraplaque hemorrhage. Intraplaque hemorrhage is an unambiguous marker of plaque vulnerability. Histopathology indicates that specimen 14 is a site of acute intraplaque hemorrhage [Table 1 and Fig. 4(a)], the other specimens are not hemorrhagic. MMS indicates that specimen 14 also exhibits a high value of $[Hb]$ (9.5 mg/mL) as assessed by DRS [Fig. 3(a)], whereas all other nonhemorrhagic specimens have relatively low $[Hb]$ values ($\leqslant$3 mg/mL). This indicates that a high concentration of hemoglobin inside the plaque, as measured by DRS, is consistent with intraplaque hemorrhage. The intraplaque hemorrhage in sample 14 was not detected by Raman spectroscopy (through the hemoglobin basis spectrum) because of the presence of calcification in the tissue. The contribution of CM dominates the Raman spectrum of specimen 14 and marginalizes the contribution from all other components.

Foam cells. The presence of superficial foam cells is associated with plaque ulceration/erosion, and their detection is important in assessing plaque vulnerability.[47] We compared the magnitude of the scattering parameter A for specimens rich in foam cells and those without foam cells. It appeared

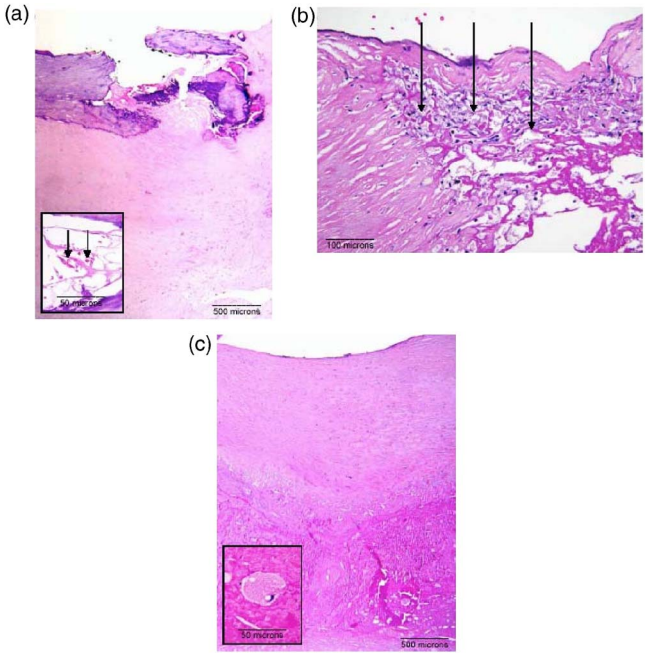

Fig. 4 Photomicrographs of representative tissue sites: (a) specimen 14, an ulcerated vulnerable plaque with acute intraplaque hemorrhage (inset; arrows indicate red blood cells) and hemoglobin fit contribution of 9.5 (mg/mL) (H and E; 4×); (b) specimen 17, a vulnerable plaque with superficial foam cells (arrows) and scattering parameter $A>2$ (H and E; 20×); and (c) specimen 9, a nonvulnerable plaque with deep foam cells (inset) and scattering parameter $A<2$ (H and E; 4×).

that a threshold value of A could serve as a parameter for assessing the presence of foam cells. To enable an accurate comparison in establishing this threshold, we only considered specimens with a relatively thick fibrous cap. Two representative specimens with superficial foam cells (11 and 12) had a mean value of A of 2.3, whereas two specimens without superficial foam cells (7 and 9) had 1.7 as the mean value of A. Based on this, a threshold value of $A=2$ was selected.

Foam cells are present in all ten specimens with $A>2$ [Fig. 3(b)], and they occur at an average depth of 250 μm below the surface of these plaques [Table 1 and Fig. 4(b)]. Foam cells are observed in only two of the seven specimens with $A<2$, and these foam cells tend to reside deeper in the plaque at an average depth of 1100 μm [Table 1 and Fig. 4(c)]. Given the range of several hundred micron sampling depth for DRS excitation wavelengths, we do not expect to sense such deep-lying foam cells; moreover, these deep-lying foam cells are not clinically relevant to plaque vulnerability. The inverse relationship of A with foam cell depth suggests that foam cells, which contain a high concentration of lipid vacuoles, are strong light scatterers and that their presence near the surface should markedly enhance tissue scattering. Thus, the intensity of scattering, as measured by DRS, can to be used to indicate the presence of superficial foam cells.

Thin fibrous cap. A thin fibrous cap is the hallmark of a vulnerable plaque. As discussed earlier, the parameter $\rho=C_{308}/C_{340}$ assesses the amount of collagen present in the top layer of tissue. A large value of ρ indicates a thinner layer. Hence, ρ can provide information about the thickness of the fibrous cap. To study this, we performed a two-layer Monte Carlo simulation in which we varied the thickness of a top collagen-rich layer, modeling the collagen that comprises the fibrous cap.[48] We assumed collimated delivery of excitation light in a uniform beam of 200 μm diam; fluorescence was generated in the tissue proportional to the fluence of the excitation light within the varied top layer. The fluorescence collected at the surface was compared for 308- and 340-nm excitation wavelengths. As expected, the ratio of the collected fluorescence excited by 308- versus 340-nm light is a monotonically decreasing function of the thickness of the fluorescing layer, asymptotically leveling off. For a 65-μm-thick layer, the value of the ratio is approximately in the middle of the range. This suggests that the value of ρ in the middle of our experimental range of ρ's can separate specimens with thin fibrous caps from those with thicker caps. We thus chose $\rho=1.8$ as the threshold value.

Indeed, of the diseased specimens (3 through 17), all those with $\rho>1.8$ (14, 15, and 16) have a minimum fibrous cap thickness well below 65 μm (Table 1), whereas the remaining diseased specimens have thicker fibrous caps. In specimen 17, the small value of ρ is not consistent with the histologically observed thin cap and associated plaque rupture. However, pathology also indicates that some portions of the fibrous cap are thick (range 0 to 280 μm), which can explain the small value of ρ. With this caveat, the parameter ρ, an indicator of the amount of collagen present in the topmost tissue layer, can be used to estimate fibrous cap thickness.

Necrotic core. When a large necrotic core is exposed to luminal blood flow following rupture of the fibrous cap, the coagulation cascade is triggered, resulting in thrombosis. We used the diagnostic parameter Σ, defined as the sum of the Raman fit coefficients for cholesterol crystals (CC) and foam cells/necrotic core (FC/NC), to assess presence of a necrotic core [Fig. 3(d)]. 11 of 14 specimens with $\Sigma>0.4$ had either a necrotic core or were rich ($\geq 2+$) in foam cells; only 1 of 3 specimens with $\Sigma<0.4$ had a necrotic core. Specimen 8 has a large necrotic core but $\Sigma<0.4$; however, this plaque has a thick fibrous cap (>440 μm), so the penetration depth of 830-nm light may not sufficiently sample the necrotic core in this case, and such a deep necrotic core is not associated with plaque vulnerability. In contrast, specimens 14 and 15 have high values of Σ but lack foam cells and necrotic core. It should be noted that these specimens are fibrotic-sclerotic plaques, demonstrating a well-developed fibrous cap but lacking a necrotic core and cholesterol crystals. Some investigators regard these as end stage plaques, in which the necrotic core may have been resorbed. Further studies will be needed to fully understand the significance of Σ, particularly in fibrotic-sclerotic plaques, but the results from this small sample set indicate the ability of Σ to detect necrotic core.

Identifying vulnerable plaques. Fibrous cap thickness is a key parameter and, taken together with the presence of necrotic core or foam cells, can serve as an indicator of plaque vulnerability. In addition, the presence of intraplaque hemorrhage by itself indicates a vulnerable plaque. For our sample set, having $\rho>1.8$ (thin fibrous cap) taken together with $A>2$ (foam cells) and/or $\Sigma>0.4$ (necrotic core) correctly identifies three of the four vulnerable plaques (14, 15, and 16). A value of $[Hb]>5$ (intraplaque hemorrhage) by itself also correctly identifies sample 14 as vulnerable. As discussed earlier, sample 17, which exhibits rupture and is vulnerable, would be missed by this identification scheme. The ability to localize small regions of thinning of the fibrous cap is under investigation. All nonatherosclerotic samples (1 and 2) and nonvulnerable plaques (3 through 13) are correctly identified as such.

5 Conclusion

This pilot study demonstrates the feasibility of using a combination of diffuse reflectance, intrinsic fluorescence, and Raman spectroscopy to detect morphological markers of vulnerable plaque. The approach is based on the correlation of parameters obtained from different spectroscopic modalities with pathology features and follows from a simple physical picture of the way light probes biological tissue. These spectroscopic parameters allow depth sensing and provide information about intraplaque hemorrhage, superficial foam cells, a thin fibrous cap, and large necrotic core, morphologic features that are associated with plaque vulnerability. In view of the small size of the sample set, these results should be considered preliminary. However, given these promising results, a larger study is warranted to establish the full potential of MMS by assessing spectral variability across many different pathologies and patients. The larger study will permit regression and statistics to be employed to validate these initial conclusions. Advances in instrumentation and the development of small-diameter side-viewing probes will enable percutaneous access to vessels and potentially provide clinically relevant information about plaque morphology. Thus, this method has the potential to guide diagnosis and treatment of atherosclerotic cardiovascular disease.

Acknowledgments

This research was conducted at the MIT Laser Biomedical Research Center under NIH grant number R01-HL-64675 and grant number P41-RR-02594.

References

1. R. Virmani, A. P. Burke, A. Farb, and F. D. Kolodgie, "Pathology of the unstable plaque," *Prog. Cardiovasc. Dis.* **44**(5), 349–356 (2002).
2. M. Rollo, T. Tartaglione, A. Pedicelli, and C. Settecasi, "Atherosclerosis of carotid and intracranial arteries," *Rays* **26**(4), 247–268 (2001).
3. R. Virmani, A. P. Burke, F. D. Kolodgie, and A. Farb, "Vulnerable plaque: the pathology of unstable coronary lesions," *J. Interv Card. Electrophysiol.* **15**(6), 439–446 (2002).
4. R. T. Lee and P. Libby, "The unstable atheroma," *Arterioscler., Thromb., Vasc. Biol.* **17**(10), 1859–1867 (1997).
5. I. J. Kullo, W. D. Edwards, and R. S. Schwartz, "Vulnerable plaque: pathobiology and clinical implications," *Ann. Intern Med.* **129**(12), 1050–1060 (1998).
6. M. Naghavi, P. Libby, E. Falk, S. W. Casscells, S. Litovsky, J. Rumberger, J. J. Badimon, C. Stefanadis, P. Moreno, G. Pasterkamp, Z. Fayad, P. H. Stone, S. Waxman, P. Raggi, M. Madjid, A. Zarrabi, A. Burke, C. Yuan, P. J. Fitzgerald, D. S. Siscovick, C. L. de Korte, M. Aikawa, K. E. Airaksinen, G. Assmann, C. R. Becker, J. H. Chesebro, A. Farb, Z. S. Galis, C. Jackson, I. K. Jang, W. Koenig, R. A. Lodder, K. March, J. Demirovic, M. Navab, S. G. Priori, M. D. Rekhter, R. Bahr, S. M. Grundy, R. Mehran, A. Colombo, E. Boerwinkle, C. Ballantyne, W. Insull, Jr., R. S. Schwartz, R. Vogel, P. W. Serruys, G. K. Hansson, D. P. Faxon, S. Kaul, H. Drexler, P. Greenland, J. E. Muller, R. Virmani, P. M. Ridker, D. P. Zipes, P. K. Shah, and J. T. Willerson, "From vulnerable plaque to vulnerable patient: a call for new definitions and risk assessment strategies: Part II," *Circulation* **108**(15), 1772–1778 (2003).
7. M. J. Kern and B. Meier, "Evaluation of the culprit plaque and the physiological significance of coronary atherosclerotic narrowings," *Circulation* **103**(25), 3142–3149 (2001).
8. P. R. Moreno and J. E. Muller, "Detection of high-risk atherosclerotic coronary plaques by intravascular spectroscopy," *J. Interv Card. Electrophysiol.* **16**(3), 243–252 (2003).
9. J. Wang, Y. J. Geng, B. Guo, T. Klima, B. N. Lal, J. T. Willerson, and W. Casscells, "Near-infrared spectroscopic characterization of human advanced atherosclerotic plaques," *J. Am. Coll. Cardiol.* **39**(8), 1305–1313 (2002).
10. P. R. Moreno, R. A. Lodder, K. R. Purushothaman, W. E. Charash, W. N. O'Connor, and J. E. Muller, "Detection of lipid pool, thin fibrous cap, and inflammatory cells in human aortic atherosclerotic plaques by near-infrared spectroscopy," *Circulation* **105**(8), 923–927 (2002).
11. K. Arakawa, K. Isoda, T. Ito, K. Nakajima, T. Shibuya, and F. Ohsuzu, "Fluorescence analysis of biochemical constituents identifies atherosclerotic plaque with a thin fibrous cap," *Arterioscler., Thromb., Vasc. Biol.* **22**(6), 1002–1007 (2002).
12. G. Zonios, L. T. Perelman, V. M. Backman, R. Manoharan, M. Fitzmaurice, J. Van Dam, and M. S. Feld, "Diffuse reflectance spectroscopy of human adenomatous colon polyps in vivo," *Appl. Opt.* **38**(31), 6628–6637 (1999).
13. B. Ye and G. S. Abela, "Beta-carotene enhances plaque detection by fluorescence attenuation in an atherosclerotic rabbit model," *Lasers Surg. Med.* **13**(4), 393–404 (1993).
14. M. A. Fitzmaurice, J. O. Bordagaray, G. L. Engelmann, R. Richards-Kortum, T. Kolubayev, M. S. Feld, N. B. Ratliff, and J. R. Kramer, "Argon ion laser-excited autofluorescence in normal and atherosclerotic aorta and coronary arteries: morphologic studies," *Am. Heart J.* **118**(5), 1028–1038 (1989).
15. C. Kittrell, R. L. Willet, C. de los Santos-Pacheo, N. B. Ratliff, J. R. Kramer, E. G. Maik, and M. S. Feld, "Diagnosis of fibrous arterial atherosclerosis using fluorescence," *Appl. Opt.* **24**, 2280–2281 (1985).
16. L. I. Deckelbaum, J. K. Lam, H. S. Cabin, K. S. Clubb, and M. B. Long, "Discrimination of normal and atherosclerotic aorta by laser-induced fluorescence," *Lasers Surg. Med.* **7**, 300–305 (1987).
17. L. I. Laifer, K. M. O'Brien, M. L. Stetz, G. R. Gindi, T. J. Garrand, and L. I. Deckelbaum, "Biochemical basis for the difference between normal and atherosclerotic arterial fluorescence," *Circulation* **80**, 1893–1901 (1989).
18. R. Richards-Kortum, A. Mehta, G. Hayes, R. Cothren, T. Kolubayev, C. Kittrell, N. B. Ratliff, J. R. Kramer, and M. S. Feld, "Spectral diagnosis of atherosclerosis using an optical fiber laser catheter," *Am. Heart J.* **118**(2), 381–391 (1989).
19. R. Richards-Kortum, R. P. Rava, M. Fitzmaurice, L. L. Tong, N. B. Ratliff, J. R. Kramer, and M. S. Feld, "A one-layer model of laser-induced fluorescence for diagnosis of disease in human tissue: applications to atherosclerosis," *IEEE Trans. Biomed. Eng.* **36**(12), 1222–1232 (1989).
20. J. J. Baraga, R. P. Rava, P. Taroni, C. Kittrell, M. Fitzmaurice, and M. S. Feld, "Laser induced fluorescence spectroscopy of normal and atherosclerotic human aorta using 306–310 nm excitation," *Lasers Surg. Med.* **10**(3), 245–261 (1990).
21. R. Richards-Kortum, R. P. Rava, M. Fitzmaurice, J. R. Kramer, and M. S. Feld, "476 nm excited laser-induced fluorescence spectroscopy of human coronary arteries," *Am. Heart J.* **122**, 1141–1150 (1991).
22. L. I. Deckelbaum, J. J. Scott, M. L. Stetz, K. M. O'Brien, and G. Baker, "Detection of calcified atherosclerotic plaque by laser-induced plasma emission," *Lasers Surg. Med.* **12**, 18–24 (1992).
23. L. Marcu, W. S. Grundfest, and J. M. I. Maarek, "Photobleaching of arterial fluorescent compounds: characterization of elastin, collagen, and cholesterol time-resolved spectra during prolonged ultraviolet irradiation," *Photochem. Photobiol.* **69**(6), 713–721 (1999).
24. J. M. I. Maarek, L. Marcu, W. J. Snyder, and W. S. Grundfest, "Time-resolved spectra of arterial fluorescent compounds: reconstruction with the Laguerre expansion technique," *Photochem. Photobiol.* **71**(2), 178–187 (2000).
25. J. Wu, M. S. Feld, and R. P. Rava, "Analytical model for extracting intrinsic fluorescence in turbid media," *Appl. Opt.* **32**(19), 3585–3595 (1993).
26. Q. G. Zhang, M. G. Muller, J. Wu, and M. S. Feld, "Turbidity-free fluorescence spectroscopy of biological tissue," *Opt. Lett.* **25**(19), 1451–1453 (2000).
27. I. Georgakoudi, B. C. Jacobson, J. Van Dam, V. Backman, M. B. Wallace, M. G. Muller, Q. Zhang, K. Badizadegan, D. Sun, G. A. Thomas, L. T. Perelman, and M. S. Feld, "Fluorescence, reflectance, and light-scattering spectroscopy for evaluating dysplasia in patients with Barrett's esophagus," *Gastroenterology* **120**(7), 1620–1629 (2001).
28. I. Georgakoudi, E. E. Sheets, M. G. Muller, V. Backman, C. P. Crum, K. Badizadegan, R. R. Dasari, and M. S. Feld, "Trimodal spectroscopy for the detection and characterization of cervical precancers in vivo," *Am. J. Obstet. Gynecol.* **186**(3), 374–382 (2002).
29. A. Mahadevan-Jansen and R. Richards-Kortum, "Raman spectroscopy for the detection of cancers and precancers," *J. Biomed. Opt.* **1**(1), 31–70 (1996).
30. E. B. Hanlon, R. Manoharan, T. W. Koo, K. E. Shafer, J. T. Motz, M. Fitzmaurice, J. R. Kramer, I. Itzkan, R. R. Dasari, and M. S. Feld, "Prospects for *in vivo* Raman spectroscopy," *Phys. Med. Biol.* **45**(2), R1–R59 (2000).
31. H. P. Buschman, G. Deinum, J. T. Motz, M. Fitzmaurice, J. R. Kramer, A. van der Laarse, A. V. Bruschke, and M. S. Feld, "Raman microspectroscopy of human coronary atherosclerosis: biochemical assessment of cellular and extracellular morphologic structures in situ," *Cardiovasc. Pathol.* **10**(2), 69–82 (2001).
32. H. P. Buschman, J. T. Motz, G. Deinum, T. J. Romer, M. Fitzmaurice, J. R. Kramer, A. van der Laarse, A. V. Bruschke, and M. S. Feld, "Diagnosis of human coronary atherosclerosis by morphology-based Raman spectroscopy," *Cardiovasc. Pathol.* **10**(2), 59–68 (2001).
33. J. T. Motz, M. Hunter, L. H. Galindo, J. A. Gardecki, J. R. Kramer, R. R. Dasari, and M. S. Feld, "Optical fiber probe for biomedical Raman spectroscopy," *Appl. Opt.* **43**(3), 542–554 (2004).
34. J. T. Motz, M. Fitzmaurice, A. Miller, S. J. Gandhi, A. S. Haka, L. H. Galindo, R. R. Dasari, J. R. Kramer, and M. S. Feld, "*In vivo* Raman spectral pathology of human atherosclerosis and vulnerable plaque," *J. Biomed. Opt.* (in press).
35. J. T. Motz, "Development of in vivo Raman spectroscopy of atherosclerosis," PhD thesis, p. 259, Harvard-MIT Division of Health Sciences and Technology (2003).
36. J. T. Motz, S. J. Gandhi, O. R. Šćepanović, A. S. Haka, J. R. Kramer, R. R. Dasari, and M. S. Feld, "Real-time Raman system for *in vivo* disease diagnosis," *J. Biomed. Opt.* **10**(3), 031113 (2005).
37. A. A. Oraevsky, S. L. Jacques, G. H. Pettit, I. S. Saidi, F. K. Tittel, and P. D. Henry, "Xecl laser ablation of atherosclerotic aorta—

optical-properties and energy pathways," *Lasers Surg. Med.* **12**(6), 585–597 (1992).
38. M. Keijzer, R. R. Richards-Kortum, S. L. Jacques, and M. S. Feld, "Fluorescence spectroscopy of turbid media—autofluorescence of the human aorta," *Appl. Opt.* **28**(20), 4286–4292 (1989).
39. A. J. Welch, C. Gardner, R. Richards-Kortum, E. Chan, G. Criswell, J. Pfefer, and S. Warren, "Propagation of fluorescent light," *Lasers Surg. Med.* **21**(2), 166–178 (1997).
40. M. G. Muller, T. A. Valdez, I. Georgakoudi, V. Backman, C. Fuentes, S. Kabani, N. Laver, Z. Wang, C. W. Boone, R. R. Dasari, S. M. Shapshay, and M. S. Feld, "Spectroscopic detection and evaluation of morphologic and biochemical changes in early human oral carcinoma," *Cancer* **97**(7), 1681–1692 (2003).
41. J. W. Tunnell, A. E. Desjardins, L. Galindo, I. Georgakoudi, S. A. McGee, J. Mirkovic, M. G. Mueller, J. Nazemi, F. T. Nguyen, A. Wax, Q. G. Zhang, R. R. Dasari, and M. S. Feld, "Instrumentation for multi-modal spectroscopic diagnosis of epithelial dysplasia," *Technol. Cancer Res. Treat.* **2**(6), 505–514 (2003).
42. J. R. Mourant, T. Fuselier, J. Boyer, T. M. Johnson, and I. J. Bigio, "Predictions and measurements of scattering and absorption over broad wavelength ranges in tissue phantoms," *Appl. Opt.* **36**(4), 949–957 (1997).
43. J. M. Schmitt and G. Kumar, "Optical scattering properties of soft tissue: a discrete particle model," *Appl. Opt.* **37**(13), 2788–2797 (1998).
44. W. H. Lawton, E. A. Sylvestre, and B. J. Youngferraro, "Statistical comparison of multiple analytic procedures—application to clinical-chemistry," *Technometrics* **21**(4), 397–409 (1979).
45. A. S. Haka, K. E. Shafer-Peltier, M. Fitzmaurice, J. Crowe, R. R. Dasari, and M. S. Feld, "Diagnosing breast cancer by using Raman spectroscopy," *Proc. Natl. Acad. Sci. U.S.A.* **102**(35), 12371–12376 (2005).
46. P. R. Bevington and D. K. Robinson, *Data Reduction and Error Analysis for the Physical Sciences*, p. xvii, p. 328, McGraw-Hill, New York (1992).
47. M. L. Higuchi, P. S. Gutierrez, H. G. Bezerra, S. A. Palomino, V. D. Aiello, J. M. Silvestre, P. Libby, and J. A. Ramires, "Comparison between adventitial and intimal inflammation of ruptured and non-ruptured atherosclerotic plaques in human coronary arteries," *Arq. Bras. Cardiol.* **79**(1), 20–24 (2002).
48. O. R. Šćepanović, M. Fitzmaurice, J. A. Gardecki, J. Nazemi, R. R. Dasari, and M. S. Feld, "Depth-sensitive information about layered tissue structures assessed by fluorescence spectroscopy," (to be published).